Effect of enzymatic *versus* titanium dioxide/silicon dioxide catalyst on crystal structure of "green" poly(butylene succinate-co-dilinoleic succinate) copolymers

Martyna Sokolowska[1], Ewa Stachowska[2], Michalina Czaplicka[2] and Miroslawa El Fray [1,*]

[1] West Pomeranian University of Technology, Szczecin, Faculty of Chemical Technology and Engineering, Department of Polymer and Biomaterials Science, Al. Piastow 45, 71-311 Szczecin, Poland

[2] Poznan University of Technology, Institute of Mechanical Technology, Division of Metrology and Measurement Systems, ul. Piotrowo 3, Poznan 60-965, Poland

*Corresponding author: mirfray@zut.edu.pl

Graphical abstract

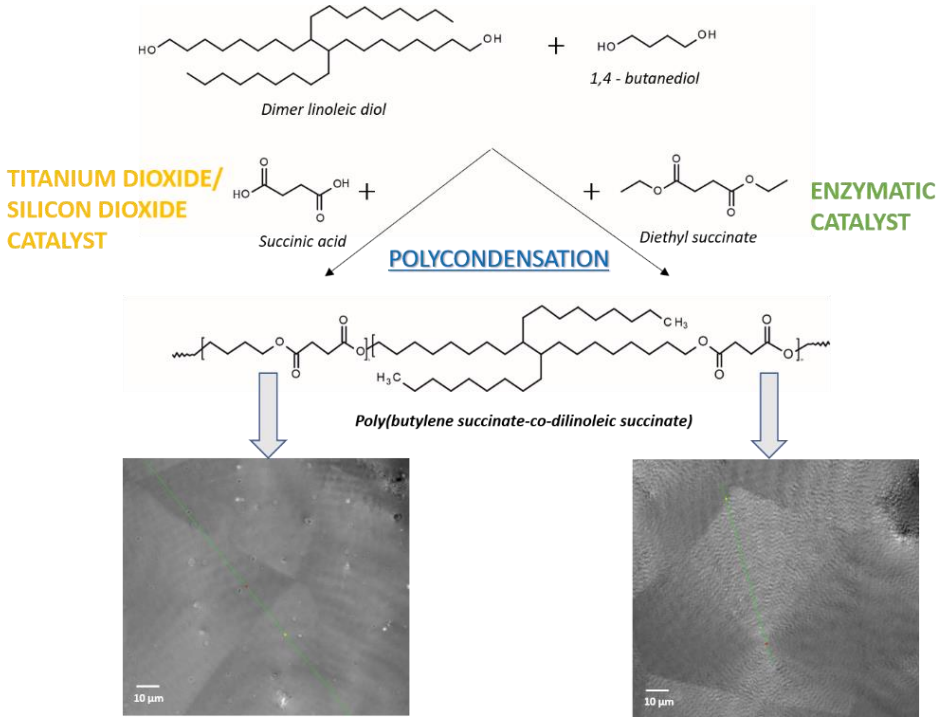

Abstract

Focusing on an eco-friendly approach, biodegradable poly(butylene succinate-co-dilinoleic succinate) (PBS-DLS) copolymers with 70:30 (wt%) ratio of hard to soft segments were successfully synthesized *via* different processes and catalytic systems. In this approach, biobased succinate was polymerized with renewable 1,4 – butanediol and dimer linoleic diol to obtain "green" copolyesters as sustainable alternative to petroleum-based materials. In the first procedure, two-step synthesis in diphenyl ether was performed using *Candida antarctica* lipase B (CAL-B) as a biocatalyst. Second material was produced *via* two-step melt polycondensation with the presence of heterogeneous titanium dioxide/silicone dioxide (C-94) catalyst. Obtained PBS-DLS copolyesters were further characterized in regard to their number average molecular weight, chemical structure, thermal transition temperatures and crystallization behavior. Here, a digital holographic microscopy has been used to study the crystallization behavior of synthesized segmented copolyesters for the first time. Using this technique, it was possible to reveal the twisting of crystalline regions in formed spherulites and observe the differences in crystallization behavior of copolyesters depending from the type of catalyst. Structural characterization indicated random and blocky structure of copolymers depending form the type of catalyst. The number average molecular weight (M_n) was noticeable higher in case of PBS-DLS 70:30 copolymer catalyzed using C-94 catalyst than PBS-DLS 70:30 synthesized with use of CAL-B. However, the degree of crystallinity was lower for polymer catalyzed with heterogeneous catalyst. Furthermore, DSC thermal analysis revealed that synthesized copolyesters exhibit low glass transition temperature as well as high melting point which is typical for thermoplastic elastomers.

Key words: enzymatic catalysis; polyesters; poly(butylene succinate); crystallization; biodegradable polymers; renewable resources; digital holographic microscopy; non-destructive testing

Introduction

In recent years, the production of biodegradable polymeric materials from renewable sources has gained enormous attention in both industrial and academic fields. It is a promising approach to solve a number of problems such as increasing pollution and energy shortage caused by the petroleum consumption (1). Among biobased materials, segmented block copolymers exhibit a broad range of advantageous features as they can be produced using monomers from biomass feedstock. These copolymers consist of different types of sequences with different properties and distinct transition temperatures, thus being capable of forming hard and soft segments. Hard segments are designed to impart dimensional, thermal and mechanical stability to the polymer. The other segments are responsible for the elastomeric properties of the material, due to low elastic modulus and glass transition temperature (T_g), and they are called soft segments. With appropriate selection of these building blocks it is possible to obtain biobased polyesters with a wide range of potential applications such as packaging, fibers, scaffolds and drug delivery systems (2–4).

Lipases are enzymes which are widely employed in the biocatalytic synthesis of polymers (5)(6–10). Among these group, *Candida antarctica* Lipase B (CAL-B) is the most popular biocatalyst, as it possesses several desirable properties such as: high regio-, chemio-, and enantioselectivity, broad substrate specificity and commercial availability. Moreover, it works well with various monomers and organic solvents under mild or slightly elevated temperature conditions. In effect, enzyme-based catalysis provides an efficient platform for developing green and sustainable polymer chemistry. This eco-friendly approach is even more appealing since both enzyme and monomers are derived from renewable resources.

It is already known that lipases can be successfully used to produce a number of polymeric materials including polyesters, polysaccharides, polyamides and polycarbonates (5,11,12). For example, Kobayashi *et al.* produced polyesters using divinyl sebacate and glycerol in the presence of unsaturated fatty acid derived from vegetal oils (13). Azim *et al.* prepared high molecular weight poly(butylene-succinate)(PBS) *via* two-stage method (14). Catalani *et al.* described azeotropic polymerization of 1,4:3,6-dianhydro-D-glucitol-based polyesters using lipase CAL-B as catalyst (15). In fact, lipases have been widely used to obtain other biobased materials such as 2,5-bis(hydroxymethyl)furan-based polyesters (16), glucose-based polyesters (17), dimer fatty acid-based polyesters (18) and polyamides (19,20).

Among all the advantages of CAL-B as catalyst, the most powerful attribute is high selectivity of this enzyme. This is mainly due to the specific structure of CAL-B and to be more precise, from the

shape of active site environment that is responsible for substrate specificity. In comparison to other lipases, CAL-B possesses an active site pocket where the available amount of space is rather limited thus, it exhibits very high regio-, enantio- and stereoselectivity (21). For example, Rogalska *et. al* showed that CAL-B exhibit higher reactivity towards smaller triglycerides with short aliphatic chain and showed strong preference for the *sn1* and *sn3* position, which indicates CAL-B typoselectivity (22). On the other hand, CAL-B exhibits high affinity for the primary hydroxy groups in the carbohydrates during acylation process. This phenomenon was not observed in case of other lipases, which showed relatively low selectivity towards primary hydroxyl groups and it strongly indicates CAL-B regioselectivity (21). Moreover, CAL-B can be a very convenient tool in modern organic chemistry due to the highly pronounced enantioselectivity. Obtaining optically pure and active compounds by using traditional methods can be very difficult to achieve and in some cases is one of the crucial tasks, for example in pharmaceutical industry. According to numerous examples found in literature, CAL-B shows increased catalytic activity towards R-enantiomer of secondary alcohols and secondary acetate which is in agreement with Kazlauskas rule, based on which it is possible to determine if the size of the substituents will be able to reach stereogenic center of the enzyme (21,23–25). Together these aspects strongly contribute to the formation of highly ordered chemical structures as well as on material homogeneity. In fact, the ability to form crystal structures is more effective.

Thus, taking into account that the enzymatic CAL-B catalyst can significantly influence crystalline structure of polymers, the aim of this study was to assess the difference in crystal structure for poly(butylene succinate-co-dilinoleic succinate) (PBS-DLS) copolymers synthesized with the use of CAL-B and heterogeneous titanium dioxide/silicone dioxide (C-94) for comparison. To our knowledge, this is the first time that digital holographic microscopy has been used to study the crystallization behavior of segmented copolyesters.

Experimental

Materials

Dichloromethane (DCM: ≥ 99.5%) and diphenyl ether (≥ 99%) were purchased from Sigma Aldrich (Poznan, Poland), diethyl succinate (DS: ≥ 99%) was purchased from SAFT (St. Louis, USA). Succinic acid (SA: ≥ 99%) and 1,4-butanediol (BD: ≥ 99%) was purchased from Alfa Aesar (Kandel, Germany). Dimer linoleic diol (DLA-OH) Pripol™ 2033 (dimer alcohol : ≥ 96.5%) was kindly provided by Croda Coatings & Polymers (Gouda, The Netherlands). Chloroform ($CHCl_3$: ≥ 98.5%) was purchased from Chempur (Piekary Slaskie, Poland), metanol (MeOH : ≥ 99.8%) was purchased from Stanlab (Lublin, Polska). Lipase B from *Candida antarctica* (CAL-B), covalently immobilized on polyacrylate beads (300-500 μm > 95%, Fermase CALB™ 10000), with a nominal activity of 10 000 PLU/g (propyl laurate Units per gram dry weight), was purchased from Fermenta Biotech Ltd. Mumbai and from Enzyme Catalyzed Polymers LLC Akron (OH, USA). Titanium dioxide/silicon dioxide

coprecipitate catalyst (C-94) was purchased from Huntsman (Germany). Diphenyl ether was stored over 4Å molecular sieves and CAL-B was pre-dried under vacuum for 24h before to use at 40 °C. The rest reagents were used as received.

Polymer synthesis with enzymatic catalyst

The following procedure was applied for the enzymatic polymerization as discussed in our previous work (5,18). Briefly, we synthesized poly(butylene succinate-co-dilinoleic succinate) with a 70:30 wt% hard to soft segments ratio catalyzed with enzyme (abbreviated as PBS-DLS 70:30_E). The dilinoleic-succinate soft segments (DLS) were built using dilinoleic diol (DLA-OH) while butylene-succinate (PBS) hard segments were built using 1,4-butanediol. Briefly, CAL-B (10 wt% of total monomers) was added to a round-bottom flask containing 1,4-butanediol (BD), diethyl succinate (DS) and dimer linoleic diol (DLA-OH) in diphenyl ether (200 wt% of total monomers). The prepared solution was placed into oil heated bath on a magnetic stirrer (Chemland). The first step was carried out under inert gas flow at atmospheric pressure and at an initial temperature of 80°C. After 1 hour, when the reaction mixture was homogeneous, the temperature was slowly increased to 95° C and the collection of ethanol was monitored until total theoretical amount of this by-product was separated (3 h). Further oligomerization was conducted under pressure of 600 Torr for 21 h, this mild vacuum was applied to prevent monomers loss due to evaporation and allow for their conversion into non-volatile oligomers. In next step, the pressure has been gently reduced to 2 Torr, while still maintaining the reaction temperature at 95 °C for 96h. Upon completion, the product mixture was dissolved in chloroform and filtered to remove catalyst. The obtained chloroform solution was added dropwise to cold methanol under continuous stirring to precipitate a white polymer product. The precipitated product was filtered, washed three times with cold methanol, collected and dried in vacuo at 40 °C for 24h.

Polymer synthesis with titanium-based catalyst

We followed the similar procedure as reported in our previous work to prepare poly(butylene succinate-co-dilinoleic succinate) with 70:30 wt% ratio of hard to soft segments using titanium-based catalyst, and abbreviated as PBS-DLS 70:30_M (26). Briefly, two-stage polymerization was performed in which 1,4 – butanediol (BD), succinic acid (SA) (molar ratio of BD to SA 1.1:1) and first aliquote of titanium dioxide/silicon dioxide catalyst (C-94)(0.06 g per 100 g of SA) were added into the reactor and copolymerized at 180°C, through an esterification reaction. This reaction was run until 95% of theoretical amount of water was separated from reaction mixture (1 h). In the next step, dimer linoleic diol (DLA-OH) and a second aliquote of C-94 catalyst were added into the reactor and further polycondensation was conducted under pressure of 0.15 – 0.3 Torr and temperature of 240 °C. Progress of reaction was measured by power consumption of the stirrer of the fully automated polycondensation unit.

Materials characterization

Chemical structure

The chemical structure of the synthesized copolymers was assessed by nuclear magnetic resonance (^{1}H and ^{13}C NMR) and Fourier transform infrared spectroscopy (ATR-FTIR). A TM Bruker DPX 400 spectrometer (400 MHz) was used to record spectra of ^{1}H NMR (128 scans, 1 second relaxation delay) and ^{13}C NMR (5120 scans, 1 relaxation delay). The samples were dissolved in $CDCl_3$ (^{1}H NMR ~ 40mg/mL, ^{13}C NMR ~ 80 mg/mL) and tetramethylsilane (TMS) was employed as internal reference for reported chemical shifts. The copolyester composition was determined from the ratio of the integrals of the signals assigned to the butylene units of PBS hard segments at 1.71 ppm (4H) and dimer linoleic diol of the DLS soft segments at 0.85 ppm (6H). The analysis of NMR spectra has also been used for molecular weight (M_n) calculation. FTIR spectra were collected using Bruker ALPHA spectrometer equipped with an Attenuated Total Reflectance (ATR) cell across the spectral range of 400 to 4000 cm^{-1} with a 2 cm^{-1} resolution. Samples were vacuum-dried prior the measurement and spectra were averaged from 32 scans.

Gel permeation chromatography

The number average molecular weight (M_n), weight average molecular weight (M_w) as well as dispersity index (Đ) were determined by GPC. Measurements were conducted in a set-up consisting of a Viscotek VE 1122 pump, column system and detector. The separation system consisted of two, 300 x 75 mm high resolution Styragel columns with a mixed bed PLgel 5 μm Mixed C (Polymer Laboratories). Chloroform with a flow rate of 1 mL/min was used as the eluent in a thermostatic system at 35 °C. In every case 100 μL of analyzed samples were injected into the chromatograph in the form of chloroform solutions with a 3% (w/v) concentration. The Shodex SE 61 differential refractometer was used as the detector. The M_n, M_w and Đ values were evaluated based on a calibration curve determined for narrow polystyrene standards.

Thermal properties

Thermal analysis of PBS-DLS 70:30 copolymers was conducted using a TA Instruments DSC Q2500 Discovery differential scanning calorimeter. Specimens were weighted (~20 mg) into aluminum pans and tightly closed before analysis. Measurements were carried out in a heating-cooling-heating cycle over the temperature range from -90 to 200 °C under nitrogen atmosphere and at heating/cooling rate of 10 °C/min. Obtained thermograms were analyzed using Trios software and the glass transition temperature (T_g) was derived as the midpoint of the transition in a second heating run.

Digital holographic microscopy

The microstructure of PBS-DLS copolymers during spontaneous crystallization was observed using a DHM T1000 digital holographic transmission microscope from Lyncée Tec (Lausanne, Switzerland) (27). The samples were sandwiched between two microscope glasses, heated to 200 °C,

and then cooled down to room temperature (24 °C). Second heating was then applied again to 200 °C. Measurements were carried during a second cooling to room temperature. The sample thickness between microscopic slides was ~10 μm. The digital microscope uses an off-axis Mach-Zehnder interferometer configuration and is equipped with a 666 nm laser diode with very low illumination power (200 μW/cm^2). The holograms were registered with a CCD camera (1024x1024 pixels, 30 fps), using a 10x objective (N.A.= 0.3; FOV= max 660 μm; no immersion) and a 40x objective (N.A.= 0.75; FOV=max 180 μm; no immersion). The lateral resolution was 0.1 μm and the axial resolution was below 1 nm. Data acquisition and evaluation were performed using the Koala Software of Lyncée Tec.

Results and discussion

In order to verify the chemical structure of obtained PBS-DLS copolyesters, materials were characterized with NMR spectroscopy. Structural analysis of ^{1}H- and ^{13}C-NMR spectra of E- and M-catalyzed PBS-DLS 70:30 copolyesters and peaks assignments are shown in Figures 1-3.

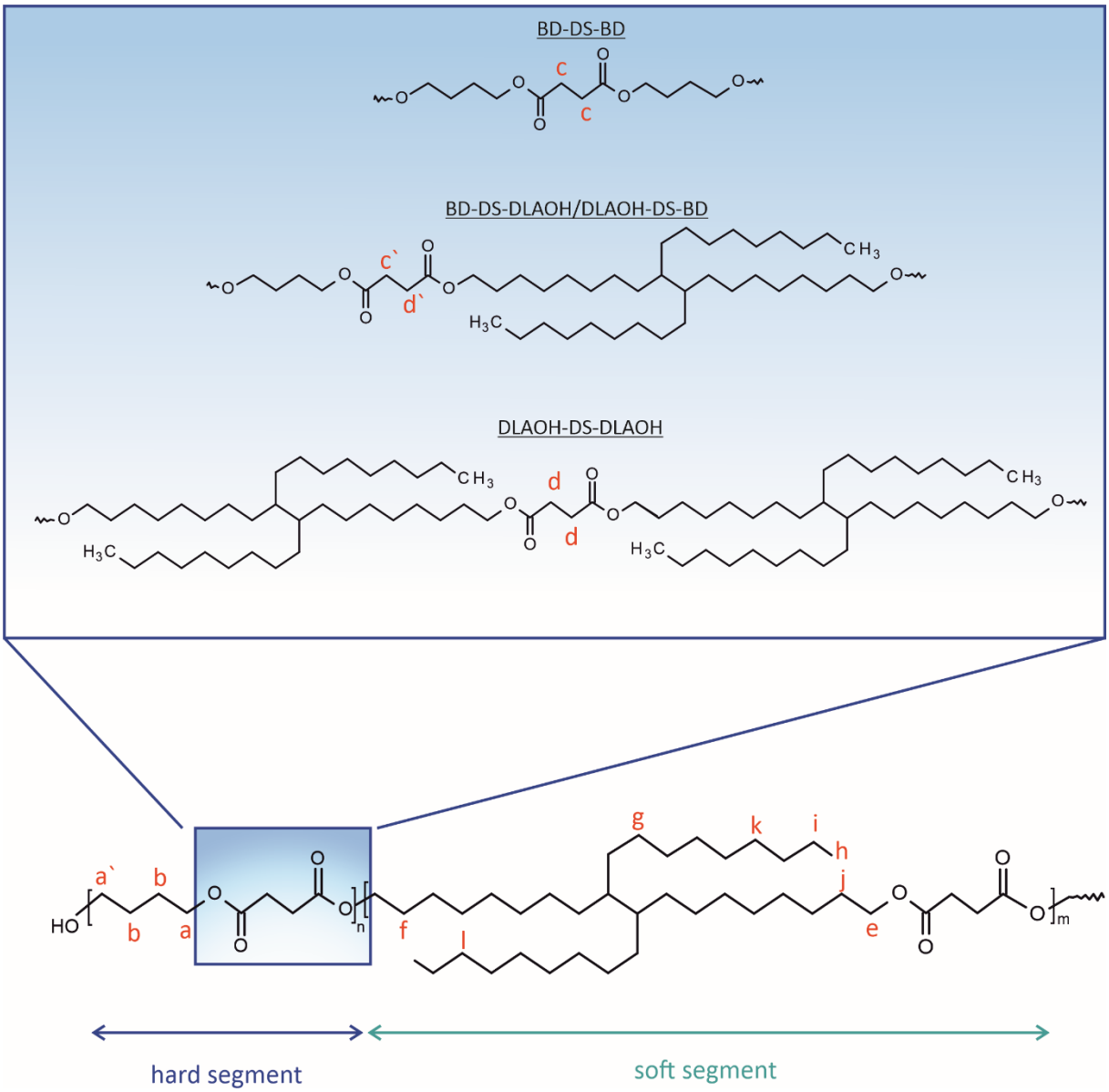

Figure 1. Chemical structure of poly(butylene succinate-co-dilinoleic succinate) (PBS-DLS) copolymers with the possible arrangements and combinations of adjacent segments, hard: butylene succinate and soft: dilinoleic succinate. Characteristic protons from ^{1}H NMR discussed in the text are marked red.

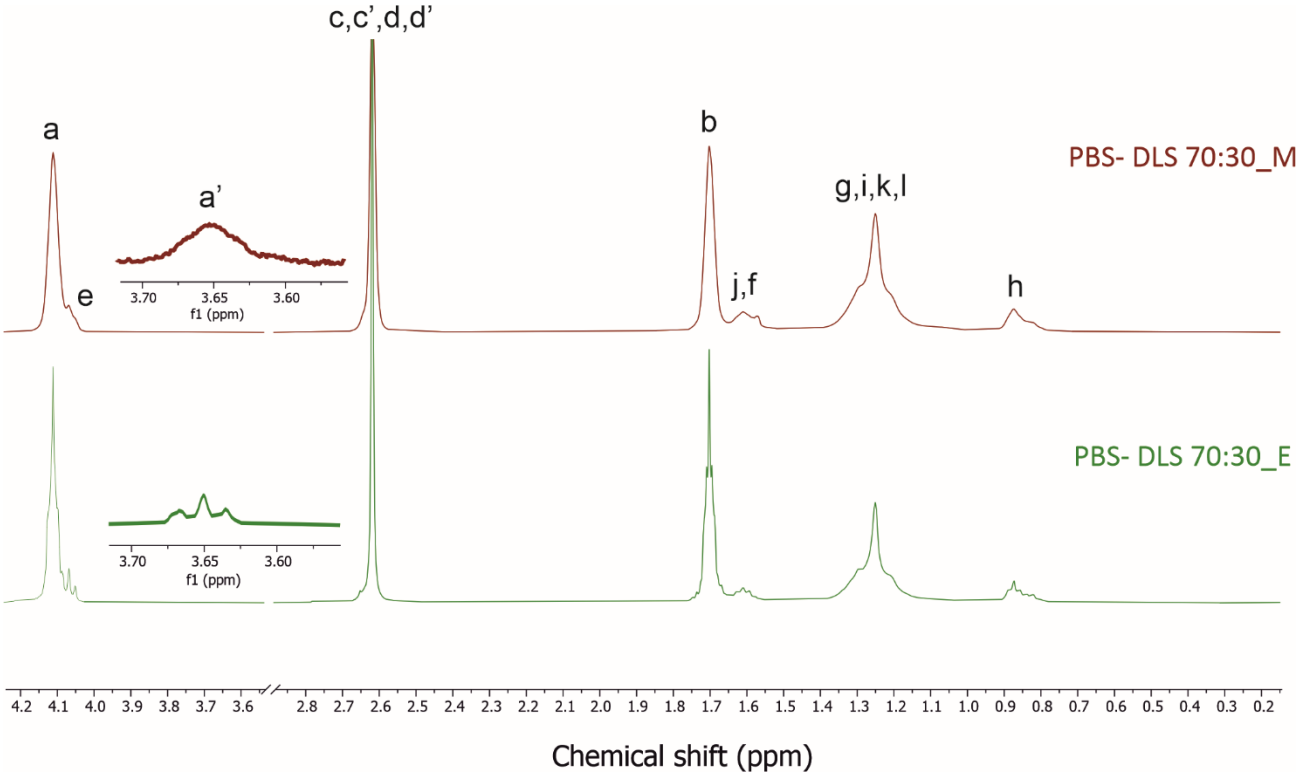

Figure 2. ^{1}H NMR spectra of PBS-DLS 70:30_E and PBS-DLS 70:30_M copolyesters.

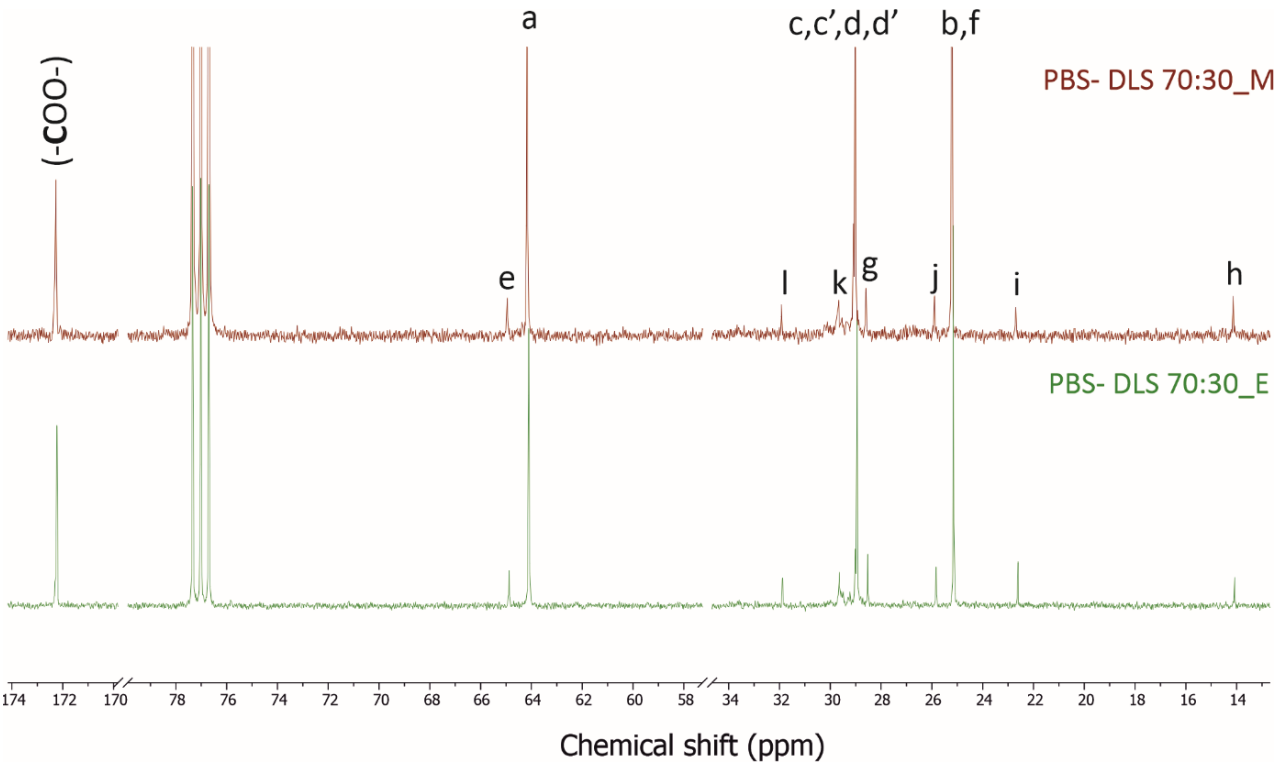

Figure 3. ^{13}C NMR spectra of PBS-DLS 70:30_E and PBS-DLS 70:30_M copolyesters.

The following signal assignments for both PBS-DLS 70:30 from ^{1}H NMR in $CDCl_3$ were registered (Fig.2). Signals located at $\delta^{1}H$ = 4.12 ppm (a) confirmed the formation of BD-DS ester bond while

signals in region (δ^1H = 4.06-4.08 ppm) (e) indicated on ester bond formation between DLA-OH and DS. Signals with low intensity resonances δ^1H = 3.66-3.69 ppm (a') are ascribed to the protons from the methylene end groups of 1,4-BD in hard segments. Methylene protons on DS and the four internal protons on 1,4-BD are located at δ^1H = 2.63 ppm (c, c', d, d') and δ^1H = 1.71 ppm (b), respectively. Finally, the six terminal protons on DLA-OH methyl end groups are located at δ^1H = 0.85 ppm (h). No residual signal were observed at the region (δ^1H = 3.61-3.64 ppm) ascribed to the unreacted hydroxyl groups of DLA-OH. Protons corresponding to the DS methylene groups at the end of the soft segments are not easily noticeable as they appear in the field around δ^1H = 4.11 ppm where the methylene units from BD are located. ^{1}H NMR analysis confirmed the expected chemical structure of PBS-DLS 70:30 copolyesters and presence of characteristic groups and bonds. No significant differences can be observed between both E- and M-PBS-DLS 70:30 samples. The incorporation of DLS segments has resulted in the appearance of signals (f), (g), (i), (j), (k), (l) and shoulder signal (e) which are not visible on the spectra of neat PBS sample presented in references (10,26).

Additionally, to obtain more detailed structural information, ^{13}C NMR measurements were performed (Fig. 3). Signal located at region δ^{13}C = 172.27 ppm is related to the DS carbon atoms from the formed carboxyl groups (-**C**OO-) attached to BD and signals arising at δ^{13}C = 25.21 ppm (b) and δ^{13}C = 29.03ppm (c) are ascribed to the -CH_2- from BD and DS units, respectively. Signal at δ^{13}C = 64.19 ppm (a) is related to the two different methylene carbons situated next to the oxygen in the ester bonds confirming the transesterification reaction between the BD and DS. On the other hand, the chemical shift located at δ^{13}C = 64.95 ppm (e) is related to the methylene carbons situated next to the oxygen in the ester bonds confirming the transesterification reaction between DLA-OH and DS. Signal detected at δ^{13}C = 14,1 (h) ppm is related to the carbons from the -CH_2**C**H_3 end-groups from DLA-OH, respectively. The chemical shift appearing at δ^{13}C = 172.30 ppm is related to the DS carbon atoms from the formed carboxyl groups (-**C**OO-) attached to the DLA-OH sequence. Signals with low intensity resonances appearing at δ^{13}C = 22.66 ppm (i), δ^{13}C = 25.85 ppm (j), δ^{13}C = 28.51 ppm (g), δ^{13}C = 29.61 (k) ppm and δ^{13}C = 31.89 (l) ppm are due to the carbon atoms from long DLA-OH aliphatic chain. This analysis confirmed the formation of the desired chemical structure of E- and M-PBS-DLS 70:30 copolyesters and the successful incorporation of DLA-OH sequences between DS units, which has resulted in the appearance of signals (e), (h), (i), (j), (k) and signals related to the carbons from DLA-OH end-groups. These chemical shifts are not visible on the spectra of neat PBS sample showed in references (10,26).

Based on the ^{1}H NMR spectra, the degree of polycondensation (DP_h) of the hard segments in PBS-DLS 70:30 copolyesters and number average molecular weight (M_n) was calculated (*see Supporting Information*).

Table 1. Sample designation, composition, degree of polymerization of hard segments, number average molecular mass calculated from ^{1}H NMR, number average molecular mass, weight average molecular mass and dispersity index calculated from GPC.

Copolymer	**Composition: wt% [mol%]**		**DP_h[a]**	**^{1}H NMR[a]**	**GPC[b]**		
	Theoretical	Calculated [a]		M_n [g/mol]	M_n [g/mol]	M_w [g/mol]	Đ
PBS-DLS 70:30_E	70/30 [89.4/10.6]	68/32 [88.6/11.4]	7.79	33 610	25 200	205 600	8.2
PBS-DLS 70:30_M		64/36 [86.7/13.3]	6.52	53 530	51 400	171 300	3.3

DP_h- degree of polymerization of hard segments (ratio of rigid units to flexible units (n/m)); M_n- number average molecular mass, M_w- weight average molecular mass, Đ- dispersity index, [a] values calculated from ^{1}H NMR [b] values determined from GPC.

The final polymer compositions (PBS-DLS wt% ratios) are presented in Table 1. A greater difference between the theoretical values and those calculated from ^{1}H NMR can be noticed for PBS-DLS 70:30_M. In both cases, however, we can observe that a greater amount of soft DLS segments has been incorporated into polymer, in comparison to the initial feed. We assume that this can be due to the removal of 1,4-BDO from reaction media during the vacuum assisted step. DLA-OH is much more difficult to be removed due to its long aliphatic chain and comparatively high molecular weight (~540 g/mol). Considering the C-94-catalyzed PBS-DLS 70:30 copolyester, the hard segment content is noticeably lower as compared to the CAL-B-catalyzed copolyester, which can be the result of slightly higher pressure and lower temperature (2 Torr, 95°C) used in enzymatic process in comparison to the C-94-catalyzed synthesis (0.15 Torr, 240°C). Thus, the risk associated with 1,4-BDO removal in this case is more limited. Moreover, higher amount of soft DLS segments within PBS-DLS 70:30_M structure leads to lower DP_h values.

The number and weight average molecular masses (abbreviated as M_n and M_w, respectively) as well as dispersity index (Đ) of PBS-DLS 70:30 copolymers were evaluated by GPC analysis. The results are presented in Table 1. In the case of PBS-DLS 70:30_M, we were able to obtain copolyester with higher molecular weight in comparison to PBS-DLS 70:30 synthesized using CAL-B catalyst (53 530 *versus* 25 200 g/mol). This indicates that the conditions applied during solvent-free, C-94-catalyzed procedure facilitate the production of polymer with increased M_n. Furthermore, focusing on the dispersity index values, it was expected to be equal or greater than 2, which is common for random process of step-growth polycondensation (14). The analysis of Đ values obtained for PBS-DLS 70:30_E exhibits higher dispersity of molar masses than PBS-DLS 70:30_M copolymer (8.2 *versus* 3.3). This phenomena can be related to the fact that CAL-B showed a tendency to produce polymer with a segmental structure that is more blocky, which may also lead to formation of macromolecules with different size and distribution

(see Table 2). Additionally, M_n value was also calculated from ^{1}H NMR analysis. As we can see, obtained results for PBS-DLS 70:30_M are in good agreement with GPC but less similarity can be observed in case of PBS-DLS 70:30_E which is also explainable due to the fact that these two methods are based on different measurement principles.

Furthermore, based on ^{13}C NMR spectra, a more detailed analysis of the segmental distribution within the copolyester structure was performed. Changes in the chemical environment of the signal appearing at δ^{13}C =172.3 ppm corresponding to the carbonyl carbon atoms due to the presence of BD or DLAOH yields four possible monomer sequences: BD-DS-BD, BD-DS-DLAOH, DLAOH-DS-BD and DLAOH-DS-DLAOH as indicated in Figure 4.

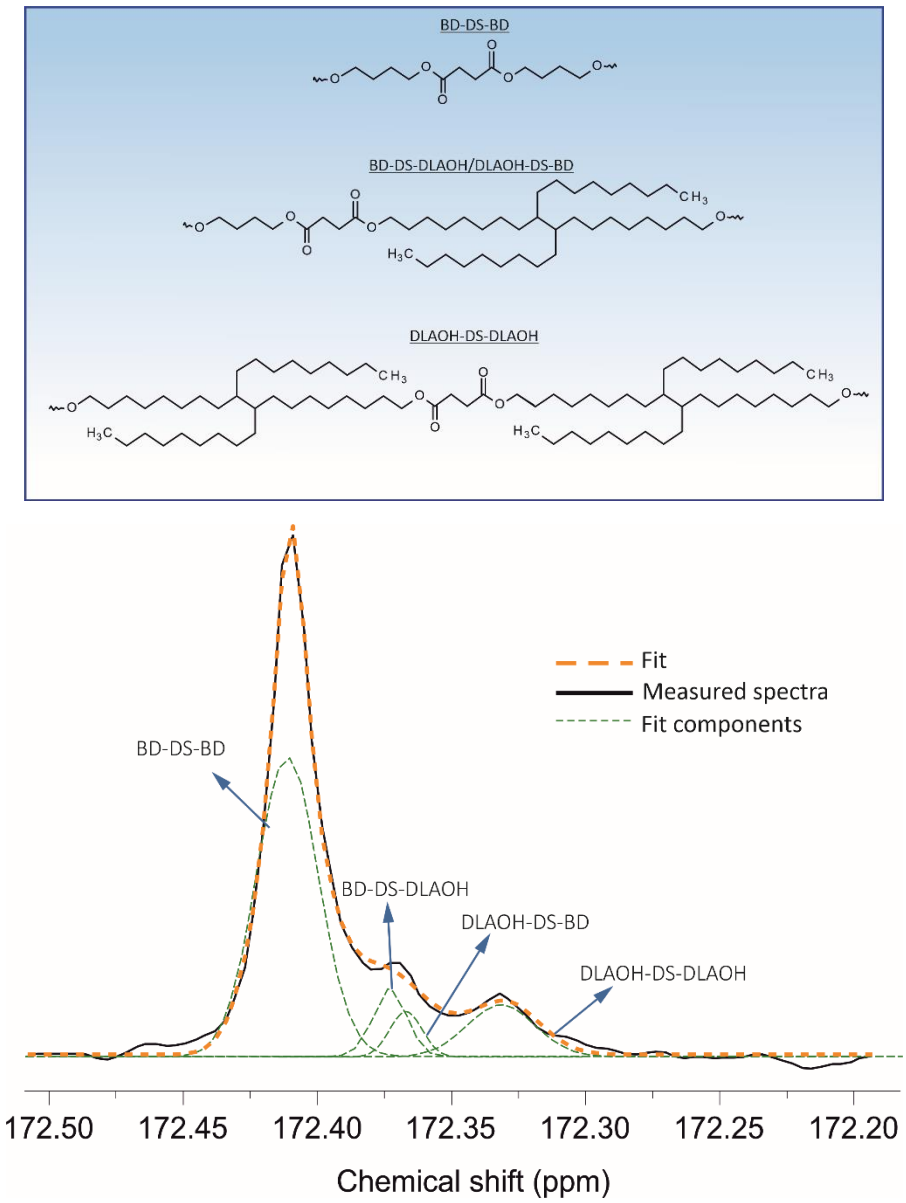

Figure 4. ^{13}C NMR spectra of the PBS-DLS 70:30_E carbonyl carbon region after deconvolution with the possible arrangements and combinations of the four triads corresponding to each peak.

After deconvolution of the signals corresponding to the characteristic carbons of carbonyl groups between two hard segments (BD-DS-BD, (172.28 ppm)), two soft segments (DLAOH-DS-DLAOH, (172.34 ppm)) and hard-soft segments (DLAOH-DS-BD/BD-DS-DLAOH, (172.3 ppm)) we were able to assess the molecular architecture, including the degree of randomness (R) and the average sequence length ($L_{BD\text{-}DS}$, $L_{DLAOH\text{-}DS}$) of hard and soft segments (in Fig. 1, these are n and m, respectively), using equations (1-3) (28):

$$L_{BD-DS} = \frac{F_{BD-DS-BD} + 0.5(F_{BD-DS-DLAOH,tot})}{0.5\ (F_{BD-DS-DLAOH,tot})} \qquad (1)$$

$$L_{DLAOH-DS} = \frac{F_{DLAOH-DS-DLAOH} + 0.5(F_{BD-DS-DLAOH,tot})}{0.5\ (F_{BD-DS-DLAOH,tot})} \qquad (2)$$

$$R = \frac{1}{L_{BD-DS}} + \frac{1}{L_{DLAOH-DS}} \qquad (3)$$

where F_x is the normalized integral value from ^{13}C NMR (x = BD-DS-DLAOH,BD-side; BD-DS-DLAOH,DLAOH-side; BD-DS-BD; DLAOH-DS-DLAOH). The results calculated for each copolymer are presented in Table 2.

Table 2. Degree of randomness and sequence segment length calculated from ^{13}C NMR.

Polymer	**R**[a]	**$L_{BD\text{-}DS}$**[b]	**$L_{DLAOH\text{-}DS}$**[b]
PBS-DLS 70:30_E	0.66	6.88	1.93
PBS-DLS 70:30_M	0.87	3.01	1.85

[a]*- degree of randomness calculated from Eq. (1);* [b]*-average sequence length calculated from Eqs. (5) and (6).*

When the degree of randomness (R) is 1, then the copolymer segments will exhibit random distribution. However, when the R values are lower than 1, then the segments have a tendency to cluster in blocks.

According to the data presented in Table 2, while the $L_{DLAOH\text{-}DS}$ values are relatively comparable for E- and M-PBS-DLS 70:30, a noticeable difference appears between $L_{BD\text{-}DS}$ values. For both copolymers, the BD-DS sequence is the longer one, but in case of PBS-DLS 70:30_E it is twice as long in comparison to PBS-DLS 70:30_M, indicating more blocky segmental distribution within the macromolecule, which is also confirmed by the calculated R-values. The R-value of the PBS-DLS 70:30_M is closer to the unity and thus, we can assume that chemical structure is more random. Use of CAL-B as catalyst leads to easier formation of BD-DS units, which can be due to the fact that the shorter building blocks can more effectively reach the region where the catalytically active site of enzyme is located. Long aliphatic chains (DS-DLS) hinder effective penetration of the CAL-B thus, limiting incorporation of these blocks into the copolymer backbone during the early synthesis stages.

Chemical structure of PBS-DLS copolyesters were further assessed by ATR-FTIR spectroscopy, as plotted in Figure 5.

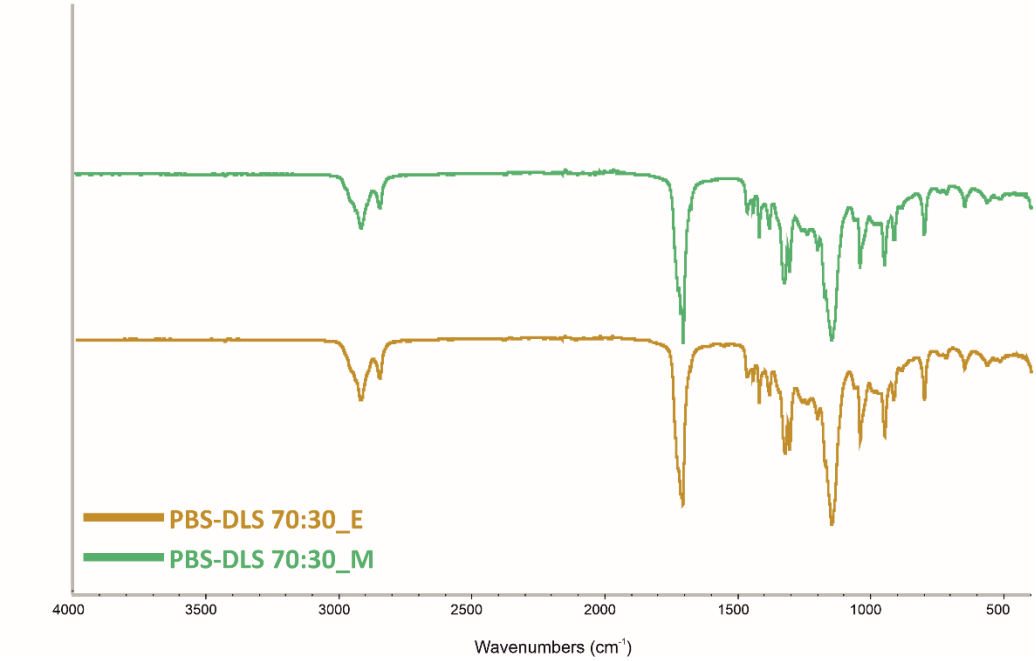

Figure 5. ATR-FTIR spectra of PBS-DLS 70:30_E and PBS-DLS 70:30_M copolymers.

Based on FTIR spectra, two peaks appearing at 2920 cm^{-1} and 2855 cm^{-1} are ascribed to the asymmetric and symmetric stretching vibrations of the -CH_2- groups in the soft DLS sequences, respectively. The strong band at 1710 cm^{-1} is assigned to the carbonyl C=O stretching vibrations. The peaks at 1210 cm^{-1} and 1150 cm^{-1} are ascribed to the asymmetric and symmetric stretching vibrations of ester C-O-C groups, respectively. Multibands appearing at 1445-1470 cm^{-1} and 1390-1425 cm^{-1} are assigned to the deformation and wagging vibration of the methylene -CH_2- groups, respectively. Bands at region 1000-500 cm^{-1} are related to the in-plane and out-of-plane deformation vibrations of aliphatic C-H and C-C groups. No significant differences were observed in the region 1700-500 cm^{-1} for the copolymer series, where the most important group appears. To conclude, FTIR analysis confirmed the expected chemical structure of PBS-DLS 70:30 copolyesters and presence of characteristic functional groups.

The combination of the rigid, crystallizable polyester segments with relatively flexible dimerized fatty acids leads to the formation of a thermo-reversible multi-phase structure that is characteristic of the thermoplastic elastomers. When the material is cooled from the melt, well-organized and crystalline domains are formed, behaving as physical crosslinks (hard segments) embedded in amorphous phase (soft segments) this is typical for such a microstructure (29). In order to evaluate phase transition temperatures and their thermal effects, DSC analysis of copolymers was performed in heating-cooling-heating cycle as described in the Materials and Methods, but only cooling and second heating measurements were taken under consideration to give comparable values. Also, the total crystalline

phase content in the polymer ($X_{c,tot}$) and crystalline phase content in the hard segments ($X_{c,h}$) were calculated using following equations (7-8):

$$X_{c,tot} = \frac{\Delta H_m}{\Delta H_m^\circ} \cdot 100\% \qquad (7)$$

$$X_{c,h} = \frac{X_{c,tot}\%}{W_H} \qquad (8)$$

where W_H is the weight content of the hard segments (PBS), ΔH_m is the melting enthalpy of the copolymer (PBS-DLS), and ΔH_m° is the melting enthalpy of 100% crystalline PBS (110.3 J/g) (30). Obtained DSC thermograms and numerical values are presented in Figure 6 and Table 3, respectively.

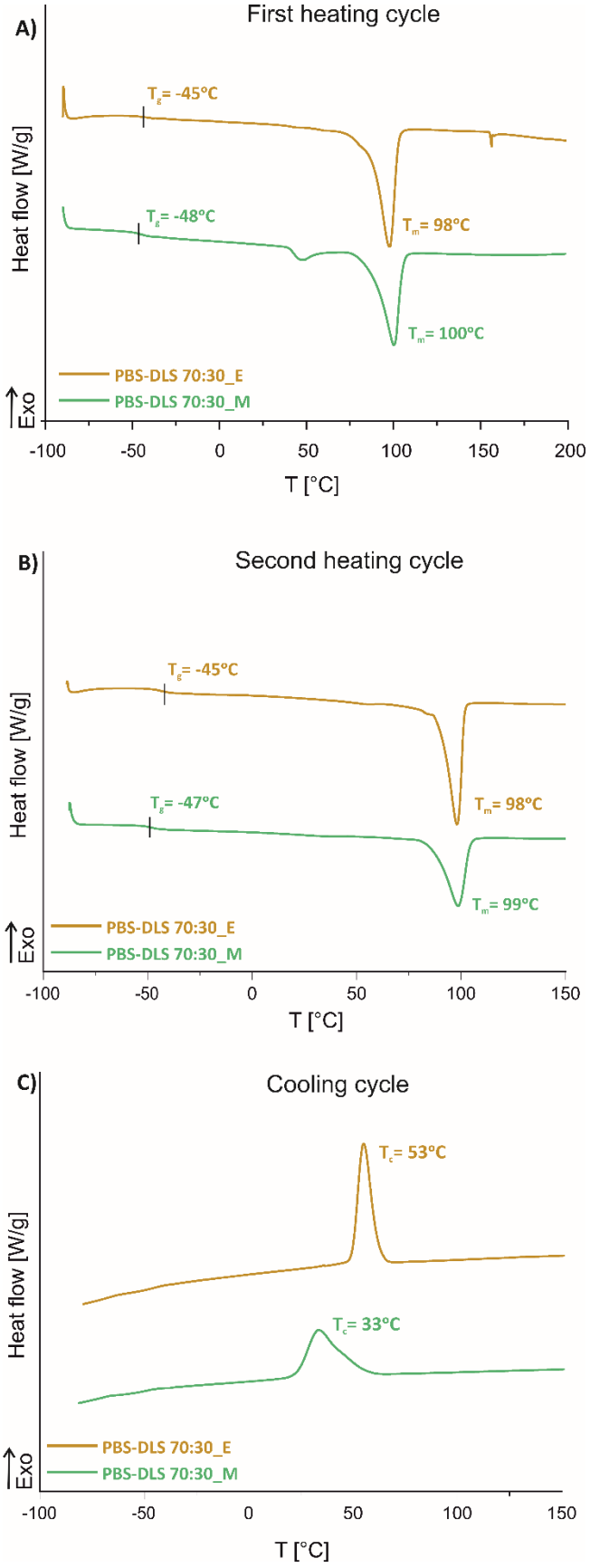

Figure 6. DSC thermograms (A) first heating cycle, (B) second heating cycle and (C) cooling cycle of the PBS-DLS 70:30 copolymer series.

Table 3. DSC results for PBS-DLS copolymer series.

Polymer	T_g [°C]	T_c [°C]	ΔH_c [J/g]	T_m [°C]	ΔH_m [J/g]	$X_{c,h}$ [%]	$X_{c,tot}$ [%]
PBS-DLS 70:30_E	-45	53	50.99	98	49.52	66.0	44.9
PBS-DLS 70:30_M	-47	33	46.09	99	44.29	62.7	40.2
PBS_E [a]	-34	70	86	110	81	-	62.0
PBS_M [b]	-34	65	62	114	54	-	49.1

T_g- glass transition temperature; ΔC_p- heat capacity at T_g; ΔH_m- melting enthalpy of the hard segments; T_m- melting temperature; T_c-crystallization temperature; $X_{c,h}$- crystalline phase content in the hard segment phase; $X_{c,tot}$- total crystalline phase content in the polymer. Both $X_{c,h}$ and $X_{c,tot}$ were computed using the actual Wh segment as determined via ^1H NMR. [a] numerical values obtained from (18), *[b] numerical values obtained from* (26).

According to data presented in Table 3 copolyesters exhibits T_g, T_m and T_c, which is typical for semicrystalline materials. Focusing on the glass transition temperature (T_g), it was shifted to lower temperatures upon incorporating the soft DLS segments for both CAL-B and C-94 catalyzed copolyesters (from -34 to -45°C and from -34 to -47°C, respectively). This indicates that amorphous phase was successfully incorporated between PBS rigid blocks, which improves material flexibility. On the other hand, the presence of soft segments hinders the crystallization transition during cooling from the melt, due to the wider distances formed between hard segments. In fact, crystallite formation and growth is less efficient, as evidenced by T_c and ΔH_c, which are shifted to the lower values after incorporation of DLS soft segments (from 70 to 53°C for PBS-DLS 70:30_E and from 65 to 33°C for PBS-DLS 70:30_M). Also, after incorporation of DLS soft segments, the quality and perfection of the crystalline phase is lower, which is reflected by a noticeable reduction in melting enthalpy (from 81 to 49.52 J/g for PBS-DLS 70:30_E and from 54 to 44.29 J/g for PBS-DLS 70:30_M). In consequence, the degree of crystallinity decreases, due to the fact that intermolecular interactions are much weaker and polymer requires less energy to melt and crystallize (31). According to the DSC results, copolyesters with the same ratio of hard to soft segments, but synthesized using different catalyst reveal a slightly different behavior. While the T_m, ΔH_m, T_g values are relatively comparable for E- and M-catalyzed PBS-DLS 70:30 copolyesters, noticeable differences appear in crystallization transition. Considering T_c values for C-94-catalyzed materials, they are shifted to lower temperatures in comparison to CALB-catalyzed copolymer (33°C versus 53°C). This phenomenon is due to the fact that PBS-DLS 70:30_E exhibits higher $X_{c,h}$ and $X_{c,tot}$ values than PBS-DLS 70:30_M (66.0 *versus* 62.7% and 44.9 *versus* 40.2%,

respectively). Also, the average sequence length of hard segments ($L_{BD\text{-}DS}$) in PBS-DLS 70:30_E is two times higher than PBS-DLS 70:30_M (6.88 *versus* 3.01). In effect, the formation of crystalline phase in PBS-DLS 70-30_E is more efficient due to the stronger intra- and/or intermolecular interactions between rigid sequences. Moreover, in case of PBS-DLS 70:30_M, the crystallization exotherm is significantly broader compared to CAL-B-catalyzed material, which indicates that the formation of crystallites with larger size-distribution and different degree of perfection.

Crystallization of copolyesters synthesized with two different catalysts was studied with digital holographic microscopy. The observed area was 128.5x128.5 μm^2.

Phase images were recorded which allowed to measure profiles along the green lines marked on the phase images (Fig.7). The vertical axis [z(deg)] refers to a phase change of the laser wave that passes through the given position of the sample. It results from different refractive indexes at different positions in the sample. The refractive index is proportional to the sample density. From the recorded profile, one can determine the difference in the phase change when the light passes through the spherulite, as compared with the phase of the beam passing through the amorphous region.

The images shown in Fig. 7 illustrate spherulite growth for PBS-DLS 70:30_E during spontaneous cooling to 24°C, which are a common polymer crystalline structures formed by radial aggregation of smaller crystals around central nuclei. The diameters of these crystalline forms increased continuously (Fig. 7 a-c), while the phase difference between amorphous and crystalline phase remained almost constant, $\Delta\varphi$ = 138 deg. In the later phase of crystallization, the round shapes of the spherulites were deformed due to the lack of space to further expand. This can also be seen in the final solid state form (Fig. 7d). The final density distribution was very homogeneous; $\Delta\varphi$ = 10 deg what can be related to high crystallinity of hard segments, $X_{c,h}$ determined from DSC (30.5%). The typical structure of the individual spherulites was however preserved. This is also shown in a 3D computer reconstruction of the last phase image presented in Fig. 8.

a)

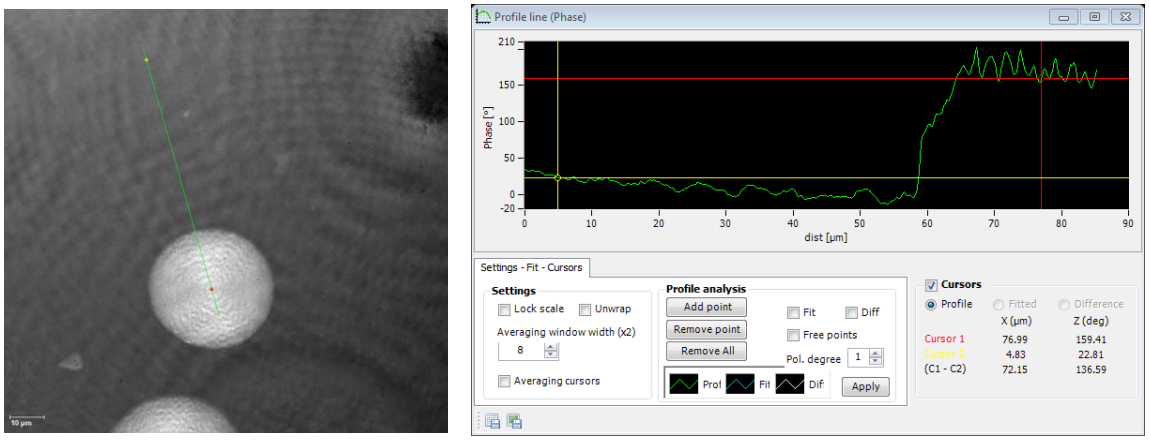

b)

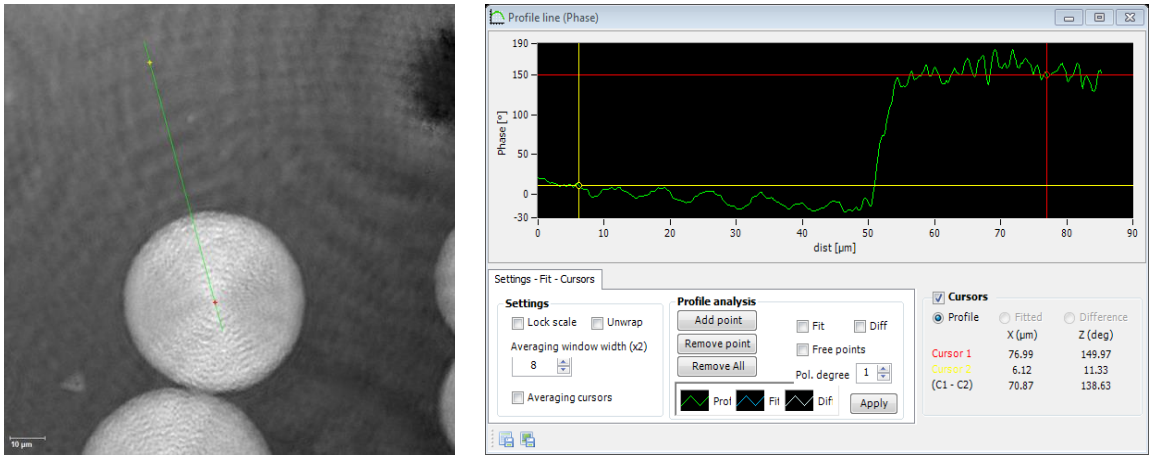

c)

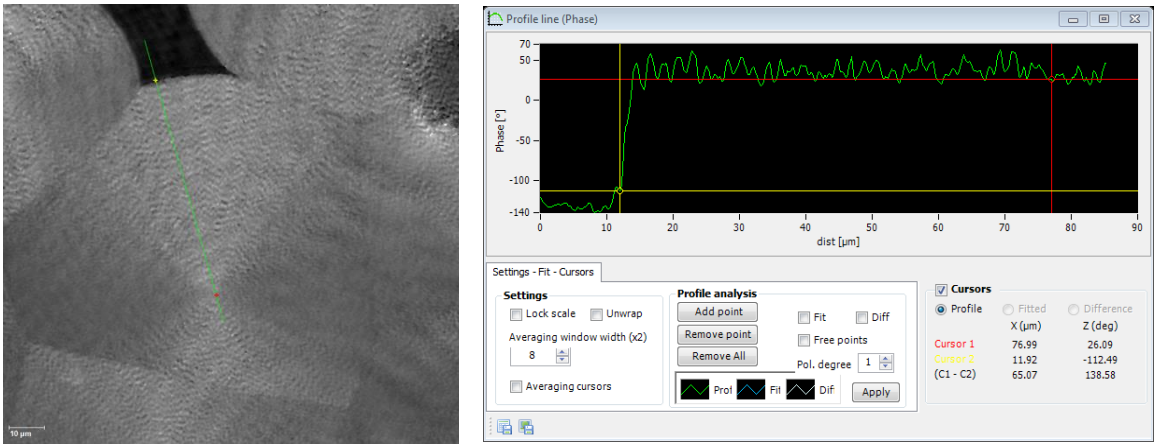

d)

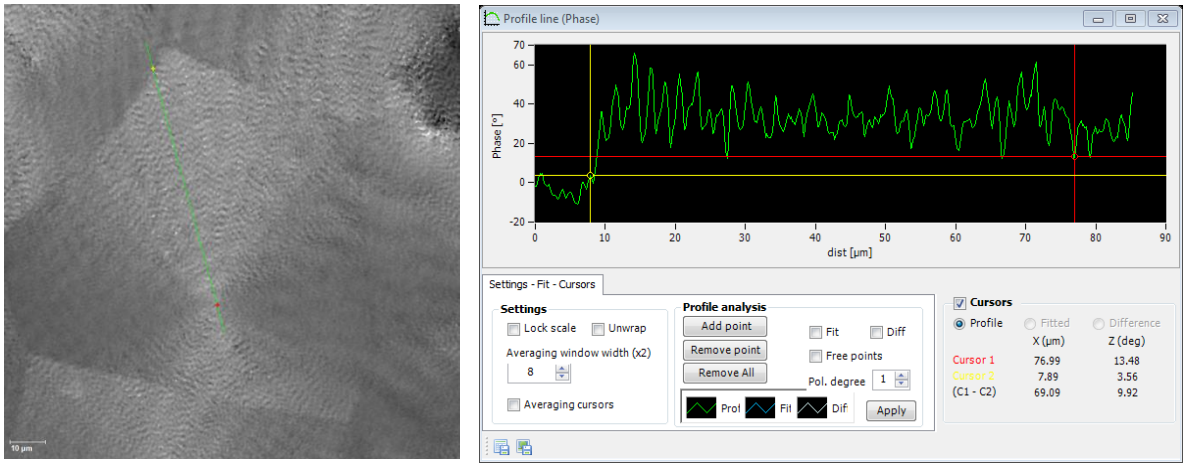

Figure 7. Holographic images for PBS-DLS 70:30_E (unwrapped phase images) and corresponding profile lines of the differences in phase along the green lines in parts a-d; magnification 40x; a: single spherulites are created; b: diameter of the spherulites increased by 20% and they start to contact; c:

further expansion of the spherulites caused their deformation due to the lack of space; d: final view: solid state.

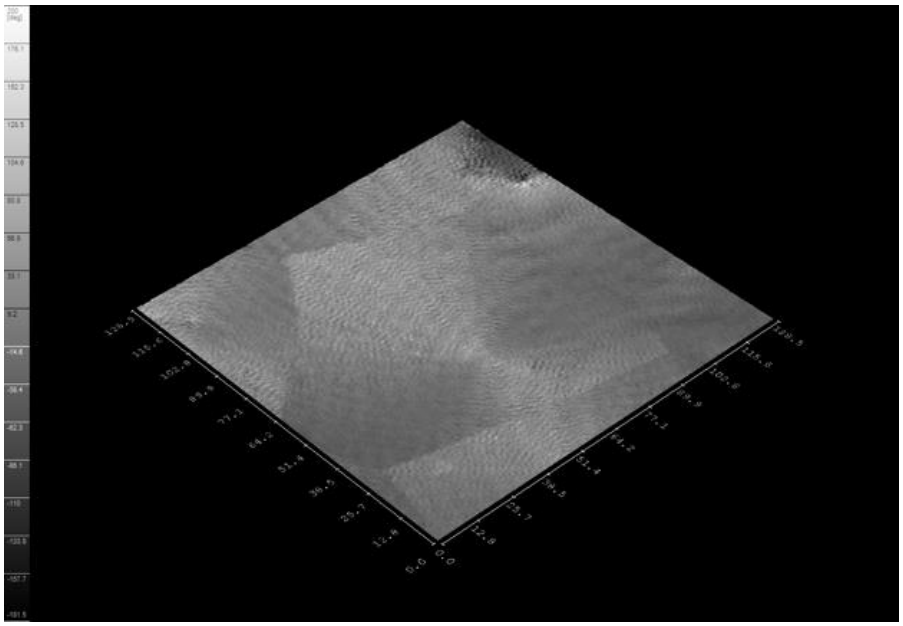

Figure 8. 3D computer reconstruction of the phase image presented in Fig. 7d. The white color corresponds to the largest phase change of the beam passing through the sample, the dark gray color to the smallest. In the xy plane, the scale is in μm, on the z-axis in deg. The area observed is 128.5x128.5 μm^2.

A different crystallization behavior was observed for PBS-DLS 70:30_M catalyzed with titanium-based catalyst (Fig. 9). The crystallizing spherulites surrounded by molten phase were more dense; the phase change $\Delta\varphi$ = 164 deg was approx. 20% greater than for PBS-DLS 70:30_E. In the center of each spherulite a characteristic peak was created, which can be ascribed to the formation of nucleation site. In the later phase of the crystallization, the spherulites were also strongly deformed due to lack of space to expand further. However, the final density distribution was much less homogeneous than for PBS-DLS 70:30_E ; $\Delta\varphi$ = 48 deg what correspond to lower crystallinity $X_{c,h}$ determined from DSC. This is also shown in a 3D computer reconstruction of the last phase image presented in Fig. 10.

a)

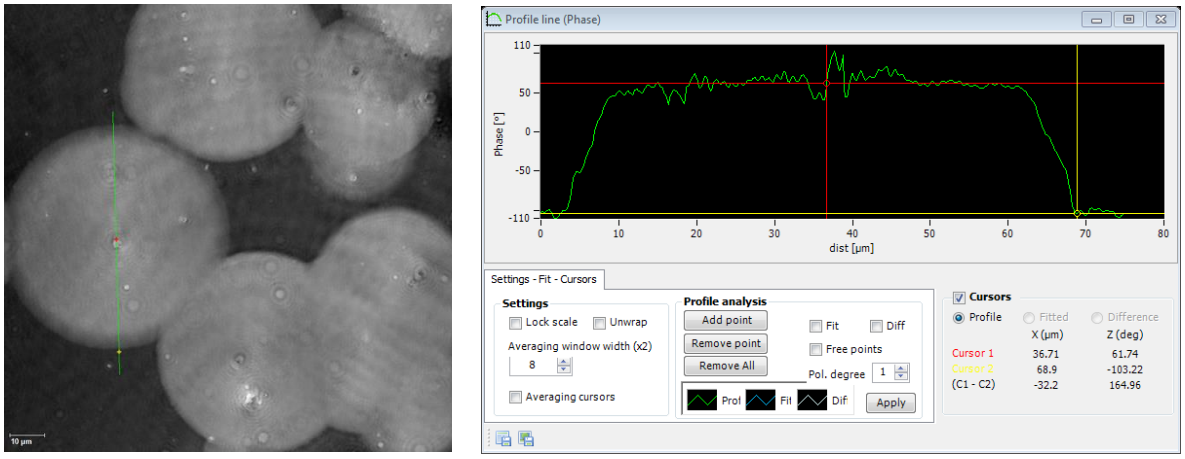

b)

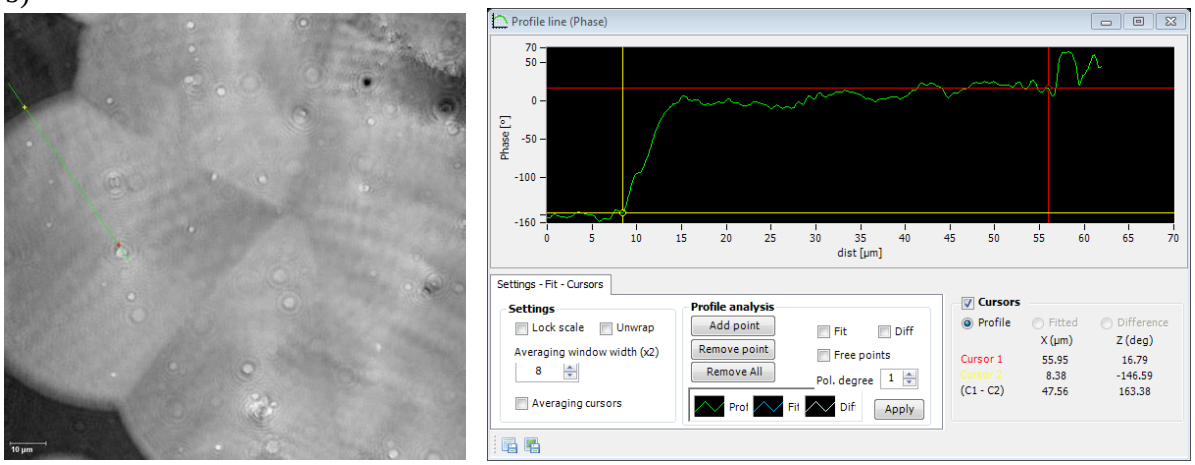

c)

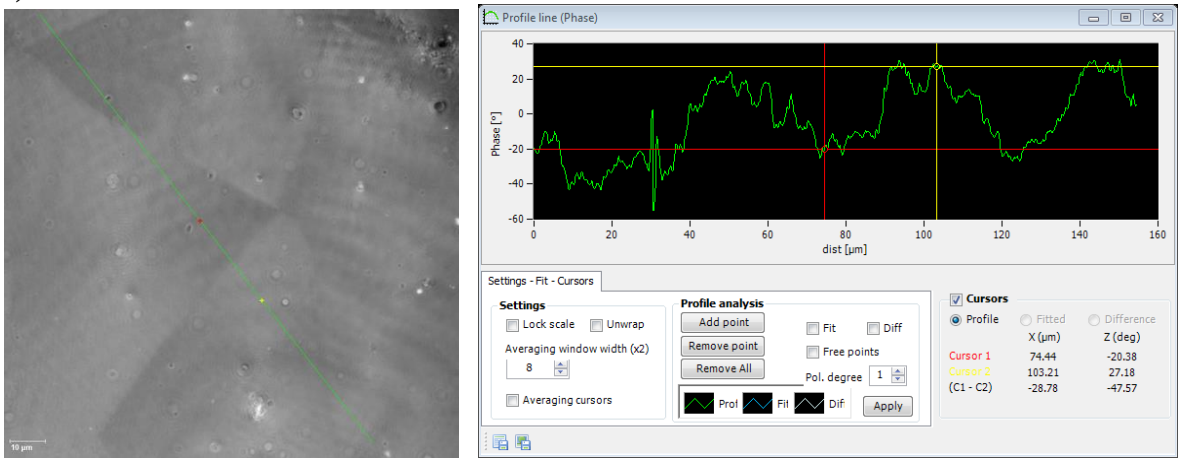

Figure 9. Microstructure and profile from the holographic microscope for a PBS-DLS 70:30_M sample crystallized from the melt.

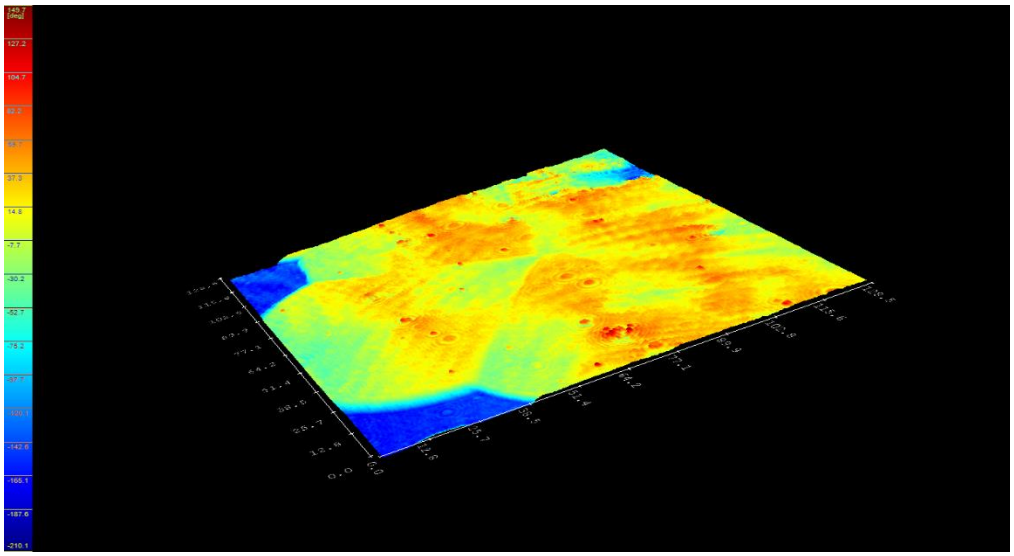

Figure 10. 3D computer reconstruction of the phase image presented in Fig. 9-c. The red color corresponds to the largest phase change of the beam passing through the sample, the dark blue color to the smallest. In the xy plane the scale is in μm, on the z-axis in deg. The area observed is 128.5x128.5 μm^2

Furthermore, we determined a change in the roughness parameter, (S_a) (expressed in deg, see Fig. 11) of PBS-DLS 70:30_E and PBS-DLS 70:30_M during spontaneous cooling with an exponential temperature decrease. The crystallization curve has a sharper signal peak for PBS-DLS 70:30_E than for PBS-DLS 70:30_M. The crystallization also started and finished at a higher temperature for PBS-DLS 70:30_E. The final roughness parameter S_a of the crystallized PBS-DLS 70:30_M was approx. two times larger, $\Delta\varphi \cong 18$ deg, than for PBS-DLS 70:30_E.

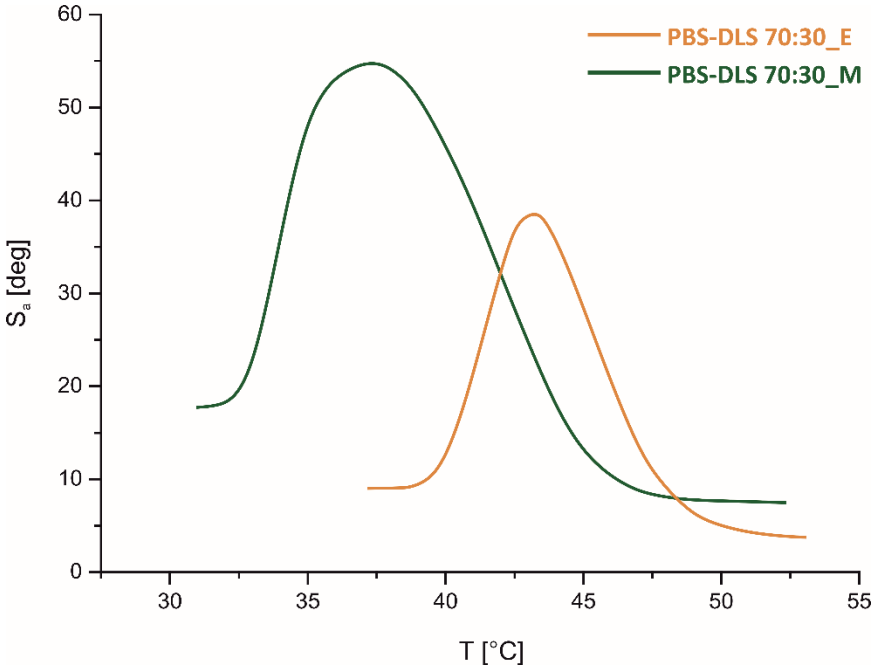

Figure 11. The roughness of the samples (S_a) during the cooling process

According to Figs. 7 and 9, spontaneous crystallization of PBS-DLS copolymers from the melt has resulted in appearance of spherulites that possess light-dark bands, indicating a twisted crystallite orientation. This phenomena is highly pronounced in optically active compounds presenting chiral conformation (32,33). In these kinds of spherulites, radially oriented crystalline forms twist jointly with right- or left-hand throughout given sectors and twist orientation of those forms is related to the unbalanced basal surface stress. Therefore, spaces between dark bands (*S*) corresponds directly to half of the twist turn period.

Banded structures of the obtained PBS-DLS may be related to the presence of dimerized fatty acids within macromolecule structure, which may form the center of chirality due to the presence of labile chains. In obtained copolyesters those long labile fragments could be responsible for the twisting crystalline orientation. (Fig. 12).

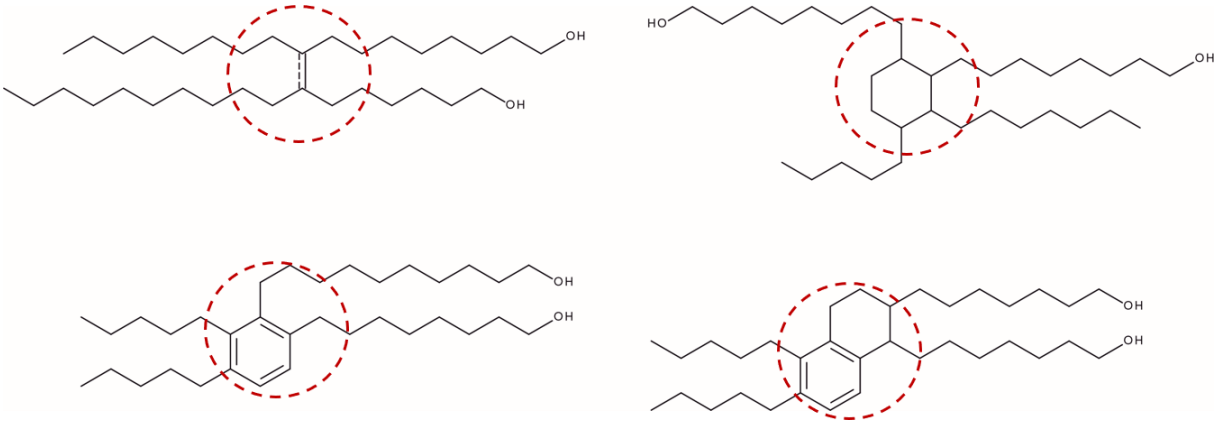

Figure 12. Possible structures of dimerized fatty acid derivative (DLA-OH, Pripol™ 2033) containing labile chains as a source of macromolecule chirality. Area with asymmetric atoms marked red dotted line.

In case of PBS-DLS 70:30_E, band periodicity is relatively small in comparison to PBS-DLS 70:30_M where well-organized banded structure can hardly be observed, which may indicate that helical chains of CAL-B-catalyzed PBS-DLS 70:30 are more twisted (Fig. 13). In PBS-DLS 70:30_E the average sequence length of hard segments ($L_{BD\text{-}DS}$), which are responsible for crystallization process is two times higher than for PBS-DLS 70:30_M (see Table 2, 6.88 *versus* 3.01). In C-94-catalyzed copolymer, incorporation of DLS amorphous segments between PBS units lead to shortening of rigid block chains thus hindering their crystallization. On the other hand, considering higher molecular mass of PBS-DLS 70:30_M copolymer, the spherulite growth rate is low and this effect is even more pronounced at low undercoolings. This can be the reason why in PBS-DLS 70:30_M the banded spherulite structure is not well developed as in case of PBS-DLS 70:30_E which is characterized by smaller M_n (see Table 1).

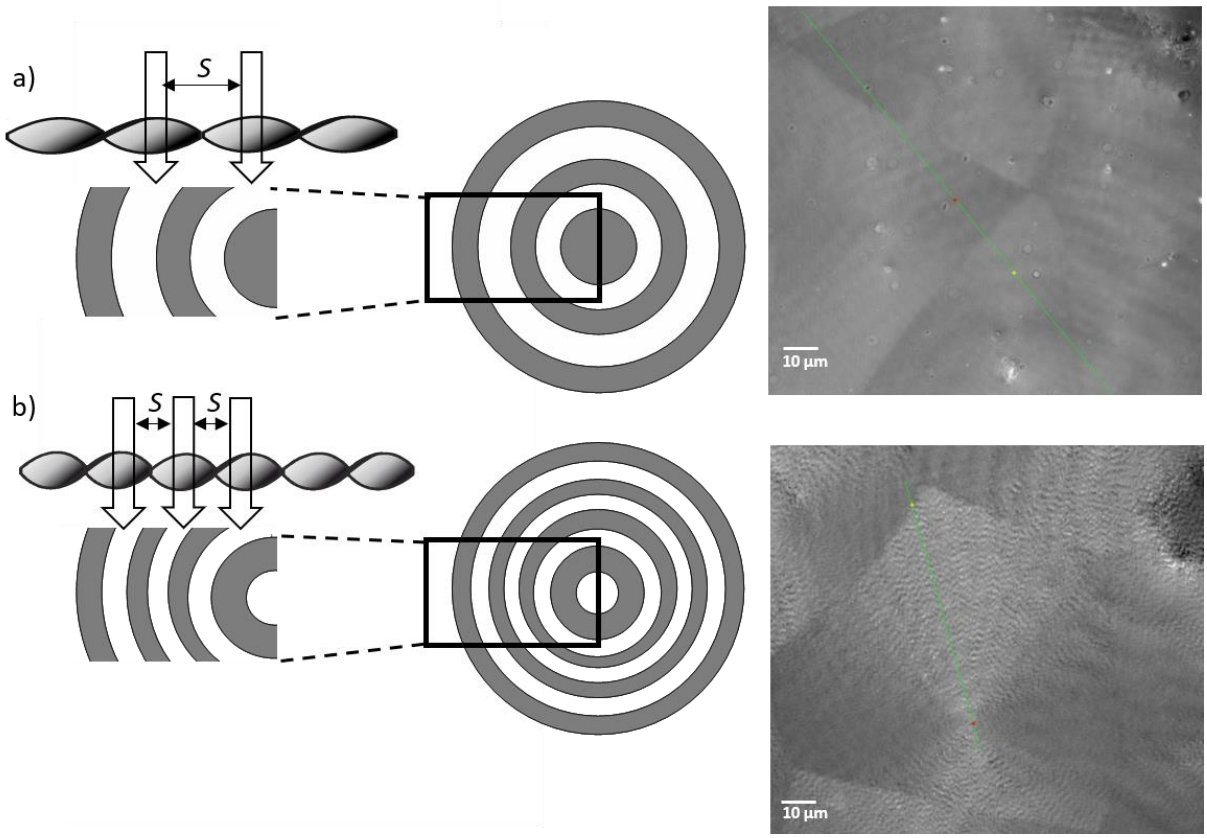

Figure 13. Scheme showing possible twisted helical chain orientation corresponding to the bright-dark fields in banded spherulites. a) PBS-DLS 70:30_M, b) PBS-DLS 70:30_E.

Conclusion

In this paper, we successfully synthesized poly(butylene succinate-co-dilinoleic succinate) PBS-DLS 70:30 copolymers using two different catalyst systems. ^{1}H NMR measurements confirmed that materials obtained were multiblock copolyesters and that the ratio of hard to soft segments was very close to 70:30 wt%. Although, average sequence length of BD-DS and DLAOH-DS units ($L_{BD\text{-}DS}$, $L_{DLAOH\text{-}DS}$) as well as degree of randomness (*R*) calculated from ^{13}C NMR, revealed that PBS-DLS 70:30_M had a more random segmental distribution within copolymer macromolecule compared to PBS-DLS 70:30_E where hard and flexible units showed tendency to cluster in blocks. GPC analysis revealed number average molecular masses to be 51 000 g/mol for C-94-catalyzed copolyester and 25 000 g/mol for CAL-B-catalyzed material. Furthermore, dispersity index has been found to be 8.2 and 3.3 for E- and M-PBS-DLS 70:30, respectively, which also proves that the synthesis method had a significant effect on the material properties.

DSC revealed two-phase morphology with low temperature glass transition (T_g) of soft segments and high melting point (T_m) of hard segments. Furthermore, lower T_c and ΔH_c values obtained for PBS-DLS 70:30 copolyesters compared to literature data for PBS homopolymer evidenced that the crystallites formation and growth is less efficient after incorporation of DLS soft segments. The

crystalline phase content in the hard segments ($X_{c,h}$) and total crystalline phase content in the polymer ($X_{c,tot}$) was higher for PBS-DLS 70:30_E than PBS-DLS 70:30_M (66.0 *versus* 62.7%, and 44.9 *versus* 40.2%, respectively).

Finally, the crystallization behavior of copolyesters synthesized with use of different catalytic systems was assessed for the first time using digital holographic microscopy. Spontaneous crystallization of PBS-DLS copolymers films from the melt resulted in appearance of banded spherulites. Differences in spherulites formation has been observed. In the case of PBS-DLS 70:30_M, crystalline forms were more dense and the phase change was approx. 20% greater than for PBS-DLS 70:30_E. However, the density distribution was more homogeneous for enzymatically catalyzed copolyester than for polymer catalyzed with heterogenous TiO_2/SiO_2 catalyst. As a consequence, the roughness parameter (S_a) of the crystallized surface was approx. two times larger for this copolyester compared to PBS-DLS 70:30_E. Furthermore, band periodicity was much smaller for PBS-DLS 70:30_E, as compared to PBS-DLS 70:30_M, which indicates that helical chains of CAL-B-catalyzed copolyester may be more twisted. Overall, this research indicated high potential of enzymatic catalysis towards PBS-DLS biobased copolyesters of uniform, highly ordered supermolecular structure.

Acknowledgments

The authors acknowledge the funding from the European Union's Horizon 2020 research and innovation program under the Marie Skłodowska-Curie grant agreement No 872152 (GREEN-MAP). MEF acknowledge financial support from Polish-U.S. Fulbright Commission grant STEM IMPACT AWARD 2019. ES acknowledges partial support by project 02/220SBAD/1501 of the Poznan University of Technology. The authors would like to thank Peter Sobolewski (West Pomeranian University of Technology, Szczecin) for help in editing the manuscript.

References

1. Hillmyer MA, Tolman WB. Aliphatic Polyester Block Polymers: Renewable, Degradable, and Sustainable. Acc Chem Res [Internet]. 2014 Aug 19;47(8):2390–6. Available from: https://pubs.acs.org/doi/10.1021/ar500121d

2. Jawad H, El Fray M, Boccaccini AR, Harding SE, Wright JS, Chen Q, et al. Nanocomposite Elastomeric Biomaterials for Myocardial Tissue Engineering Using Embryonic Stem Cell-derived Cardiomyocytes. Adv Eng Mater [Internet]. 2010 Dec;12(12):B664–74. Available from: http://doi.wiley.com/10.1002/adem.201080078

3. Jiang Y, Woortman AJJ, Alberda van Ekenstein GOR, Loos K. Enzyme-catalyzed synthesis of unsaturated aliphatic polyesters based on green monomers from renewable resources. Biomolecules. 2013;3(3):461–80.

4. Penczek P, Czub P, Pielichowski J. Unsaturated Polyester Resins: Chemistry and Technology. In 2005. p. 1–95. Available from: http://link.springer.com/10.1007/b136243

5. Sonseca A, El Fray M. Enzymatic synthesis of an electrospinnable poly(butylene succinate-co-dilinoleic succinate) thermoplastic elastomer. RSC Adv. 2017;7(34):21258–67.

6. Azim H, Dekhterman A, Jiang Z, Gross RA. Candida antarctica Lipase B-Catalyzed Synthesis of Poly (butylene succinate): Shorter Chain Building Blocks Also Work. 2006;3093–7.

7. Jiang Y, Woortman AJJ, Alberda van Ekenstein GOR, Loos K. A biocatalytic approach towards sustainable furanic–aliphatic polyesters. Polym Chem [Internet]. 2015;6(29):5198–211. Available from: http://xlink.rsc.org/?DOI=C5PY00629E

8. Stavila E, Alberda van Ekenstein GOR, Woortman AJJ, Loos K. Lipase-Catalyzed Ring-Opening Copolymerization of ε-Caprolactone and β-Lactam. Biomacromolecules [Internet]. 2014 Jan 13;15(1):234–41. Available from: https://pubs.acs.org/doi/10.1021/bm401514k

9. Skoczinski P, Espinoza Cangahuala MK, Maniar D, Albach RW, Bittner N, Loos K. Biocatalytic Synthesis of Furan-Based Oligomer Diols with Enhanced End-Group Fidelity. ACS Sustain Chem Eng [Internet]. 2020 Jan 21;8(2):1068–86. Available from: https://pubs.acs.org/doi/10.1021/acssuschemeng.9b05874

10. Jiang Y, Woortman AJJ, Alberda Van Ekenstein GOR, Loos K. Environmentally benign synthesis of saturated and unsaturated aliphatic polyesters via enzymatic polymerization of biobased monomers derived from renewable resources. Polym Chem. 2015;6(30):5451–63.

11. Kobayashi S, Makino A. Enzymatic Polymer Synthesis: An Opportunity for Green Polymer Chemistry. Chem Rev [Internet]. 2009 Nov 11;109(11):5288–353. Available from: https://pubs.acs.org/doi/10.1021/cr900165z

12. Ikeda R, Uyama H, Kobayashi S. Novel Synthetic Pathway to a Poly(phenylene oxide). Laccase-Catalyzed Oxidative Polymerization of Syringic Acid. Macromolecules [Internet]. 1996 Jan;29(8):3053–4. Available from: https://pubs.acs.org/doi/10.1021/ma951810b

13. Tsujimoto T, Uyama H, Kobayashi S. Enzymatic Synthesis of Cross-Linkable Polyesters from Renewable Resources. Biomacromolecules [Internet]. 2001 Mar;2(1):29–31. Available from: https://pubs.acs.org/doi/10.1021/bm000097h

14. Azim H, Dekhterman A, Jiang Z, Gross RA. Candida a ntarctica Lipase B-Catalyzed Synthesis of Poly(butylene succinate): Shorter Chain Building Blocks Also Work. Biomacromolecules [Internet]. 2006 Nov;7(11):3093–7. Available from: https://pubs.acs.org/doi/10.1021/bm060574h

15. Juais D, Naves AF, Li C, Gross RA, Catalani LH. Isosorbide Polyesters from Enzymatic Catalysis. Macromolecules [Internet]. 2010 Dec 28;43(24):10315–9. Available from:

https://pubs.acs.org/doi/10.1021/ma1013176

16. Jiang Y, Woortman AJJ, Alberda van Ekenstein GOR, Petrović DM, Loos K. Enzymatic Synthesis of Biobased Polyesters Using 2,5-Bis(hydroxymethyl)furan as the Building Block. Biomacromolecules [Internet]. 2014 Jul 14;15(7):2482–93. Available from: https://pubs.acs.org/doi/10.1021/bm500340w

17. Lavilla C, Alla A, Martínez de Ilarduya A, Muñoz-Guerra S. High Tg Bio-Based Aliphatic Polyesters from Bicyclic <scp>d</scp> -Mannitol. Biomacromolecules [Internet]. 2013 Mar 11;14(3):781–93. Available from: https://pubs.acs.org/doi/10.1021/bm301854c

18. Sonseca A, McClain A, Puskas JE, El Fray M. Kinetic studies of biocatalyzed copolyesters of poly(butylene succinate)(PBS)containing fully bio-based dilinoleic diol. Eur Polym J [Internet]. 2019;116(February):515–25. Available from: https://doi.org/10.1016/j.eurpolymj.2019.04.038

19. Jiang Y, Loos K. Enzymatic Synthesis of Biobased Polyesters and Polyamides. Polymers (Basel) [Internet]. 2016 Jun 25;8(7):243. Available from: http://www.mdpi.com/2073-4360/8/7/243

20. Frampton MB, Zelisko PM. Synthesis of lipase-catalysed silicone-polyesters and silicone-polyamides at elevated temperatures. Chem Commun [Internet]. 2013;49(81):9269. Available from: http://xlink.rsc.org/?DOI=c3cc45380d

21. Anderson EM, Larsson KM, Kirk O. One Biocatalyst–Many Applications: The Use of Candida Antarctica B-Lipase in Organic Synthesis. Biocatal Biotransformation [Internet]. 1998 Jan 11;16(3):181–204. Available from: http://www.tandfonline.com/doi/full/10.3109/10242429809003198

22. Rogalska E, Cudrey C, Ferrato F, Verger R. Stereoselective hydrolysis of triglycerides by animal and microbial lipases. Chirality [Internet]. 1993;5(1):24–30. Available from: http://doi.wiley.com/10.1002/chir.530050106

23. Yang B, Lihammar R, Bäckvall J. Investigation of the Impact of Water on the Enantioselectivity Displayed by CALB in the Kinetic Resolution of δ-Functionalized Alkan-2-ol Derivatives. Chem – A Eur J [Internet]. 2014 Oct 13;20(42):13517–21. Available from: https://onlinelibrary.wiley.com/doi/abs/10.1002/chem.201404233

24. Kazlauskas RJ, Weissfloch ANE, Rappaport AT, Cuccia LA. A Rule To Predict Which Enantiomer of a Secondary Alcohol Reacts Faster in Reactions Catalyzed by Cholesterol Esterase, Lipase from Pseudomonas cepacia, and Lipase from Candida rugosa. J Org Chem. 1991;56(8):2656–65.

25. Raza S. Enantioselectivity in Candida antarctica lipase B: A molecular dynamics study. Protein Sci [Internet]. 2001 Feb 1;10(2):329–38. Available from: http://doi.wiley.com/10.1110/ps.33901

26. Stępień K, Miles C, McClain A, Wiśniewska E, Sobolewski P, Kohn J, et al. Biocopolyesters of Poly(butylene succinate) Containing Long-Chain Biobased Glycol Synthesized with Heterogeneous Titanium Dioxide Catalyst. ACS Sustain Chem Eng [Internet]. 2019 Jun 17;7(12):10623–32. Available from: https://pubs.acs.org/doi/10.1021/acssuschemeng.9b01191

27. https://www.lynceetec.com.

28. Yamadera R, Murano M. The determination of randomness in copolyesters by high resolution nuclear magnetic resonance. J Polym Sci Part A-1 Polym Chem [Internet]. 1967 Sep;5(9):2259–68. Available from: http://doi.wiley.com/10.1002/pol.1967.150050905

29. Kwiatkowska M, Kowalczyk I, Kwiatkowski K, Szymczyk A, Jędrzejewski R. Synthesis and structure – property relationship of biobased poly(butylene 2,5-furanoate) – block – (dimerized

fatty acid) copolymers. Polymer (Guildf) [Internet]. 2017 Nov;130:26–38. Available from: https://linkinghub.elsevier.com/retrieve/pii/S0032386117309655

30. Correlo VM, Boesel LF, Bhattacharya M, Mano JF, Neves NM, Reis RL. Properties of melt processed chitosan and aliphatic polyester blends. Mater Sci Eng A [Internet]. 2005 Aug;403(1–2):57–68. Available from: https://linkinghub.elsevier.com/retrieve/pii/S0921509305004338

31. Mincheva R, Delangre A, Raquez J-M, Narayan R, Dubois P. Biobased Polyesters with Composition-Dependent Thermomechanical Properties: Synthesis and Characterization of Poly(butylene succinate- co -butylene azelate). Biomacromolecules [Internet]. 2013 Mar 11;14(3):890–9. Available from: https://pubs.acs.org/doi/10.1021/bm301965h

32. Saracovan I, Keith HD, Manley RSJ, Brown GR. Banding in Spherulites of Polymers Having Uncompensated Main-Chain Chirality. Macromolecules [Internet]. 1999 Dec;32(26):8918–22. Available from: https://pubs.acs.org/doi/10.1021/ma9911602

33. Crist B, Schultz JM. Polymer spherulites: A critical review. Prog Polym Sci [Internet]. 2016 May;56:1–63. Available from: https://linkinghub.elsevier.com/retrieve/pii/S0079670015001288